

Growth Substrate- and Phase-Specific Expression of Biphenyl, Benzoate, and C₁ Metabolic Pathways in *Burkholderia* *xenovorans* LB400

V. J. Denef, M. A. Patrauchan, C. Florizone, J. Park, T. V. Tsoi, W. Verstraete, J. M. Tiedje and L. D. Eltis
J. Bacteriol. 2005, 187(23):7996. DOI:
10.1128/JB.187.23.7996-8005.2005.

Updated information and services can be found at:
<http://jb.asm.org/content/187/23/7996>

REFERENCES

These include:

This article cites 42 articles, 22 of which can be accessed free at: <http://jb.asm.org/content/187/23/7996#ref-list-1>

CONTENT ALERTS

Receive: RSS Feeds, eTOCs, free email alerts (when new articles cite this article), [more»](#)

Information about commercial reprint orders: <http://journals.asm.org/site/misc/reprints.xhtml>
To subscribe to to another ASM Journal go to: <http://journals.asm.org/site/subscriptions/>

Growth Substrate- and Phase-Specific Expression of Biphenyl, Benzoate, and C₁ Metabolic Pathways in *Burkholderia xenovorans* LB400

V. J. Denef,^{1,3} M. A. Patrauchan,² C. Florizone,² J. Park,¹ T. V. Tsoi,¹ W. Verstraete,³ J. M. Tiedje,¹ and L. D. Eltis^{2*}

Center for Microbial Ecology, Michigan State University, East Lansing, Michigan 48824¹; Department of Microbiology and Immunology, University of British Columbia, Vancouver V6T 1Z3, Canada²; and Laboratory of Microbial Ecology and Technology, Ghent University, Ghent, Belgium³

Received 5 July 2005/Accepted 14 September 2005

Recent microarray experiments suggested that *Burkholderia xenovorans* LB400, a potent polychlorinated biphenyl (PCB)-degrading bacterium, utilizes up to three apparently redundant benzoate pathways and a C₁ metabolic pathway during biphenyl and benzoate metabolism. To better characterize the roles of these pathways, we performed quantitative proteome profiling of cells grown on succinate, benzoate, or biphenyl and harvested during either mid-logarithmic growth or the transition between the logarithmic and stationary growth phases. The Bph enzymes, catabolizing biphenyl, were ~16-fold more abundant in biphenyl- versus succinate-grown cells. Moreover, the upper and lower *bph* pathways were independently regulated. Expression of each benzoate pathway depended on growth substrate and phase. Proteins specifying catabolism via benzoate dihydroxylation and catechol *ortho*-cleavage (*ben-cat* pathway) were approximately an order of magnitude more abundant in benzoate- versus biphenyl-grown cells at the same growth phase. The chromosomal copy of the benzoyl-coenzyme A (CoA) (*box_C*) pathway was also expressed during growth on biphenyl: *Box_C* proteins were approximately twice as abundant as Ben and Cat proteins under these conditions. By contrast, proteins of the megaplasmid copy of the benzoyl-CoA (*box_M*) pathway were only detected in transition-phase benzoate-grown cells. Other proteins detected at increased levels in benzoate- and biphenyl-grown cells included general stress response proteins potentially induced by reactive oxygen species formed during aerobic aromatic catabolism. Finally, C₁ metabolic enzymes were present in biphenyl-grown cells during transition phase. This study provides insights into the physiological roles and integration of apparently redundant catabolic pathways in large-genome bacteria and establishes a basis for investigating the PCB-degrading abilities of this strain.

Since its isolation two decades ago, *Burkholderia xenovorans* LB400 (3, 12) has been the focus of physiological, biochemical, and genetic studies to elucidate the basis of its potent polychlorinated biphenyl (PCB)-degrading capacities (1, 3, 7, 14, 22, 27, 34, 35, 43). Such studies have established that PCBs are cometabolized by the *bph* pathway, which is responsible for the catabolism of biphenyl, and helped establish *B. xenovorans* LB400 as a model organism for understanding the aerobic biotransformation of PCBs. Nevertheless, many critical aspects of the bacterium's response to PCBs remain unknown. These include the degradation of the resulting chlorinated intermediates, such as benzoates, the involvement of other physiological processes in responding to these pollutants, and the coordinated regulation of these processes.

An analysis of the genome sequence revealed that LB400 contains two pathways, one of which is present in two copies, responsible for the aerobic catabolism of benzoate. The best characterized of these, the *ben-cat* pathway, involves two dioxygenases that catalyze the dihydroxylation of benzoate and

the *ortho*-cleavage of catechol, respectively (Fig. 1A). A second pathway, which involves a single dioxygenase that catalyzes the dihydroxylation of benzoyl-coenzyme A (CoA), is present in two copies, located on the chromosome (*box_C*) and megaplasmid (*box_M*), respectively (Fig. 1A). Exploratory transcriptomics studies (8) suggest that these pathways are expressed in a substrate-dependent manner: the *ben-cat* pathway was expressed in benzoate-grown cells, while the chromosomal *box_C* pathway was expressed in biphenyl-grown cells. Moreover, the studies confirmed the *bph* pathway (Fig. 1B) was induced during growth on biphenyl, consistent with one published report, but not another (2, 24). Finally, it was revealed that C₁ metabolic pathways were induced upon transition towards stationary phase.

In the current study, we analyzed the proteomes of benzoate- and biphenyl-grown cells using quantitative two-dimensional (2D) gel electrophoresis. The primary objective of this study was to determine the roles of each of the three benzoate-catabolic pathways as a function of carbon source and growth phase. In addition, we investigated the factors inducing the C₁ metabolic pathways. Finally, we analyzed which other cellular processes were involved in aerobic degradation of benzoate and biphenyl.

* Corresponding author. Mailing address: Department of Microbiology and Immunology, University of British Columbia, 300-6174 University Blvd., Vancouver, British Columbia V6T 1Z3, Canada. Phone: (604) 822 0042. Fax: (604) 822 6041. E-mail: leltis@interchange.ubc.ca.

MATERIALS AND METHODS

Bacterial strains and genome sequence. *Burkholderia xenovorans* strain LB400 was originally isolated from a PCB-contaminated New York state landfill site (3).

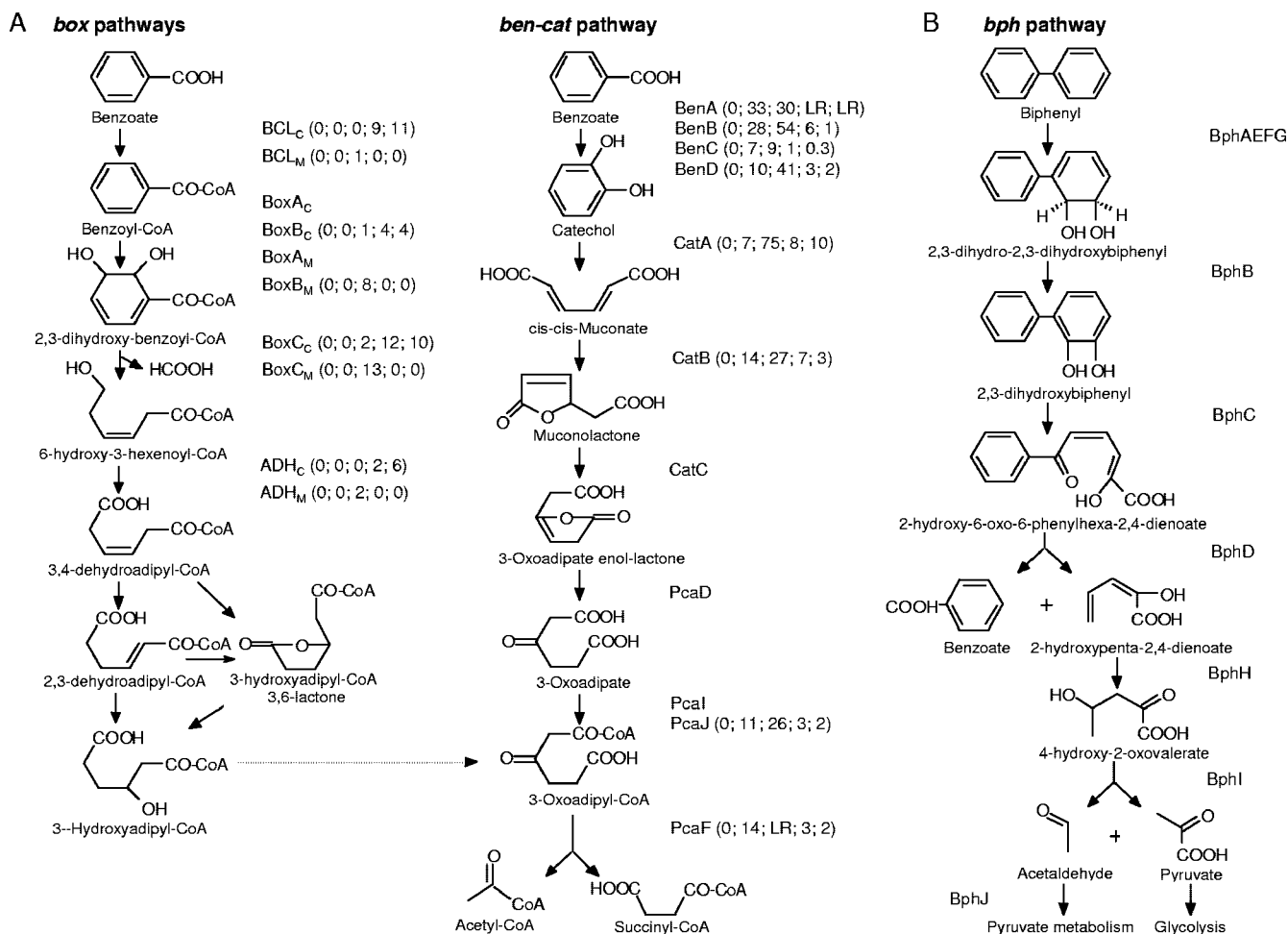


FIG. 1. (A) The two different benzoate pathways in LB400. The benzoyl-CoA pathway is present in two copies: one on the chromosome (*box_C*) and one on the megaplasmid (*box_M*). Proteins that have been linked with a particular reaction are indicated. For proteins identified in this study, molecular weight-corrected normalized volumes are given for each of five physiological states: Succ-ML; Benz-ML; Benz-TP; Biph-ML; and Biph-TP. A value of 0 means the protein spot was not detected in that condition. LR indicates poor resolution in the area where that spot was expected. (B) The biphenyl pathway in LB400. The full protein names are as follows: BCL, benzoate-CoA ligase; BoxBA, benzoyl-CoA oxygenase/reductase; BoxC, benzoyl-CoA-dihydrodiol lyase; ADH, aldehyde dehydrogenase; BenABC, benzoate 1,2-dioxygenase (large, small, and reductase subunits); BenD, *cis*-1,2-dihydroxycyclohexa-3,5-diene-1-carboxylate dehydrogenase; CatA, catechol 1,2-dioxygenase; CatB, muconate cycloisomerase; CatC, muconolactone δ -isomerase; PcaD, 3-oxoadipate enol-lactonase; PcaIJ, 3-oxoadipate CoA-transferase subunits A and B; PcaF, β -ketoadipyl-CoA thiolase; BphAEFG, biphenyl dioxygenase (large, small, ferredoxin, and ferredoxin reductase subunits); BphB, biphenyl-dihydrodiol dehydrogenase; BphC, 2,3-dihydroxybiphenyl 1,2-dioxygenase; BphD, 2-hydroxy-6-oxo-6-phenylhexa-2,4-dienoate hydratase; BphH, 2-hydroxypenta-2,4-dienoate hydratase; BphI, 4-hydroxy-2-oxovalerate aldolase; and BphJ, acetaldehyde dehydrogenase.

The whole genome sequence was produced by the Department of Energy's Joint Genome Institute and automatically annotated by Oak Ridge National Laboratory's Computational Genomics Group. The latest sequence and draft analysis are available at http://genome.jgi-psf.org/finished_microbes/burfu/burfu.home.html.

Media and growth conditions. LB400 was grown in liquid K1 mineral medium (41) supplemented with succinate (10 mM), benzoate (5 mM) particulate biphenyl (5 mM, $S = 6.99$ mg/liter) or phenylacetate (5 mM). Cells were grown in 200 ml medium in 500-ml Erlenmeyer flasks at $29 \pm 1^\circ\text{C}$ on a rotary shaker at 250 rpm. For proteomics, three biological replicates were grown as described (8) then harvested in the appropriate growth phase by centrifugation for 10 min at $16,887 \times g$ at 25°C . The cell pellets were flash frozen in liquid nitrogen and stored at -80°C . Succinate-, benzoate-, biphenyl-, and phenylacetate-grown cells were harvested in mid-log phase (Succ-ML, Benz-ML, Biph-ML, Phaa-ML, respectively). Biphenyl- and benzoate-grown cells were also harvested from cultures in the transition phase between logarithmic growth and stationary phase (Biph-TP and Benz-TP).

Preparation of cell extracts and two dimensional gel electrophoresis. All procedures were performed as described earlier (30) based on previously de-

scribed methods (10, 11). Briefly, cell pellets were washed three times with saline (0.14 M NaCl), once with TE buffer (10 mM Tris/HCl, 1 mM EDTA, pH 8.0), and stored as aliquots at -80°C . To prepare the protein extract, the pelleted cells were amended with a small amount of lysis buffer (4% cholamidopropyltrimethylammonio propanesulfate [CHAPS], 30 mM Tris, pH 7.5, protease inhibitor cocktail [one tablet of Mini Complete per 10 ml solution; Roche]; 1:100 [vol/vol]) and were disrupted using a Fast Prep Bio 101 Thermo Savant bead beater for five cycles of 15 s, speed 6.0. Unbroken cells and debris were removed and the cell-free protein extract thus obtained was either stored at -80°C or used immediately for proteomic studies. Protein concentration was determined using the 2D Quant kit (Amersham Biosciences).

After protein extraction, 2D gels were run for each of three biological replicates for LB400 cells grown on succinate (mid-log phase), benzoate (mid-log and transition phase), or biphenyl (mid-log and transition phase). Samples originated from the same cultures used in the microarray analysis described by Denef et al. (8) except for the Benz-TP and Biph-TP samples. Most of the cytosolic proteins resolved using broad-pH-range immobilized pH gradient (IPG) strips lie in the range of pI 4 to 8. To increase the resolution, each sample was analyzed using two narrow-pH-range strips, pI 3 to 7 and 6 to 9. The first-dimension separation

was carried out using nonlinear IPG strips (24 cm, pH 3 to 7 or pH 6 to 9). The pH 3 to 7 IPG strips were rehydrated "in-gel" using 90 mg protein extract resuspended in 400 ml rehydration solution (10 M urea, 2 M thiourea, 30 mM dithiothreitol, 3% CHAPS, Pharmalyte pH 3 to 10). The pH 6 to 9 IPG strips were rehydrated in the rehydration buffer and then loaded with 150 mg protein using a cup. To minimize carbamylation, the temperature was maintained between 20 and 25°C during protein solubilization.

Isoelectric focusing in the IPG strips was carried out for a total of 73.5 kVh for pH 3 to 7 IPG strips and 98 kVh for pH 6 to 9 at 20°C under mineral oil using ETTAN IPGphor (Amersham Biosciences). The IPG strips were then equilibrated and run into 12% sodium dodecyl sulfate (SDS)-polyacrylamide gel electrophoresis (PAGE) gels (24 by 20 cm) using the ETTAN DALTtwelve system (Amersham Biosciences). Broad-range molecular mass markers (Invitrogen) were run on each side of the gel. Protein was detected using Sypro Ruby, and the gels were imaged using a variable mode imager Typhoon 9400 (excitation 488 nm, emission 610 nm; Amersham Biosciences).

Analysis of 2D gels and protein identification. The 2D gel images were differentially analyzed using Progenesis Workstation software (Nonlinear Dynamics, Durham, NC). The signal intensity of each spot was averaged over gels obtained from three different cultures. Averaged gels included only proteins spots that were present in at least two of three replicate gels. Only spots with a minimum normalized volume of 0.002 or greater were analyzed further. For proteins appearing on the gel as a horizontal series of spots, likely due to carbamylation, the pI and mass of only the major spot in the series were recorded, and the difference in abundance was calculated based on the summed signal intensities of all the spots in the series. Protein spots whose intensities were at least twofold higher or lower versus the control (succinate-grown cells) were recorded as more or less abundant, respectively.

Spots of interest were excised from Sypro Ruby-stained gels and digested in-gel using trypsin (16). Mass spectrometry analyses were performed using a Voyager DESTR matrix-assisted laser desorption ionization-time of flight (MALDI-TOF) (Applied Biosystems). Proteins were identified as described previously (30) using the MASCOT search engine (www.matrixscience.com) and a database generated by in silico digestion of the total LB400 proteome predicted from the genome sequence. A protein was considered identified if the hit fulfilled four criteria: the hit was statistically significant (a MASCOT search score above 52 for the LB400 database); the number of matched peptides was 5 or higher; the protein sequence coverage was above 20%; and the predicted mass and pI values were consistent with the experimentally determined ones. When two or more significant hits were returned, it was usually possible to narrow the identification to a single hit based on listed criteria (e.g., the pI and mass of some hits did not match that of the spot). Otherwise, the identification was excluded from the data set.

To better estimate the protein relative abundance, we corrected the normalized volumes of the proteins for their mass. Molecular weight-corrected normalized volumes (NV_c) were calculated as follows: $NV_c = (NV/\text{molecular weight}) \times 1,000$, where NV is the normalized volume as calculated in Progenesis and molecular weight is the molecular weight of the protein expressed in kDa. Finally, quantification of protein using 2D gels has several limitations, including nonlinear relationships between spot volumes and protein amounts (28). The accuracy of the Progenesis normalization algorithm and linearity of signal response were verified over a limited range of total protein loaded (two- to fourfold).

RESULTS

Global summary of differential protein expression. The cytosolic proteomes of benzoate- and biphenyl-grown cells were analyzed using a 2D electrophoresis-based approach. Five different physiological states were investigated: the mid-log growth phase of cells grown using biphenyl, benzoate, or succinate (control) as the sole source of energy and carbon as well as biphenyl- and benzoate-grown cells in transition between the logarithmic growth and stationary phases. The growth rates (r) of Succ-ML, Benz-ML, and Biph-ML cells were 0.40, 0.27, and 0.23 cell divisions/h, respectively. Biph-TP and Benz-TP sampling points were chosen to maximize the physiological similarities between the cells, although this transition phase was different in the two cultures.

Biph-TP, previously identified as early stationary phase (8), samples were harvested within 3 h (less than one exponential phase generation time) after the cessation of logarithmic growth at an optical density at 600 nm (OD_{600}) of ~ 0.7 . At this point, biphenyl crystals were still visible in the medium and the cells continued growing slowly to a final density OD_{600} of 1.2. Transcriptomic studies revealed no clear starvation response in this phase (8). Benz-TP samples were harvested immediately prior to cessation of growth at an OD_{600} of ~ 0.96 . This point was chosen to avoid a strong starvation response: cultures growing on benzoate consumed essentially all of the growth substrate and underwent a short transition phase. Thus, Biph-TP and Benz-TP cells were still growing but were likely in a state of hunger. Averaged gels run over pH ranges of 3 to 7 and 6 to 9 contained approximately 1,140 and 700 protein spots, respectively (see Fig. 2 for representative gel sections). The comparative analyses described in the next two paragraphs were performed using the pH 3 to 7 gels to avoid biases due to the overlap between the two pH ranges while maximizing coverage of the proteome.

At mid-log phase, cells growing on each of succinate, benzoate and biphenyl shared approximately 60% of their detected proteomes (Fig. 3A). In pairwise comparisons, the proteomes of Biph-ML and Succ-ML cells were least similar to each other. This is consistent with the chemical properties that benzoate shares with succinate (both are organic acids) and biphenyl (both are aromatic compounds). Indeed, half of the biphenyl carbon skeleton is catabolized via benzoate and benzoate is catabolized via succinyl-CoA (Fig. 1A). Quantitative comparison of spot intensities revealed that of the 845 protein spots common to the Biph-ML and Benz-ML proteomes, 30% were at least twofold more abundant than in Succ-ML samples.

During growth on either biphenyl or benzoate, approximately 63% of the detected protein spots that were present in samples harvested at mid-log were also present in those harvested during transition phase. Moreover, approximately 45% of the spots were common to all four proteomes (Fig. 3B). On the other hand, proteomes of Biph-ML and Benz-ML cells shared 69% of their spots, indicating that the physiological states of the cells is a greater determinant of the proteome than the specific carbon source. The proteomes of the Biph-TP and Benz-TP samples only shared 56% of their spots, and each sample contained many unique spots ($\sim 30\%$). The relatively low similarity of their proteomes likely reflects the different natures of the transition phase during growth on these two compounds.

To characterize the expression of the enzymes involved in the catabolism of biphenyl and benzoate under different growth conditions, we selected 137 protein spots for identification by MALDI-TOF analysis. These protein spots fulfilled three criteria: (i) were significantly more abundant during growth on one of the aromatic compounds versus succinate; (ii) had pI and mass consistent with the predicted pI and mass of the proteins of interest; and (iii) were abundant enough for successful mass spectrometry (MS) analysis (NV above 0.01). Of these, 74% had a peptide mass spectrum profile with a significant match in the in silico LB400 proteome, some of which represented the same protein. The identified proteins include 65 that fulfilled the criteria summarized in the Material and Methods (Tables 1 and 2) and an additional 12 that only

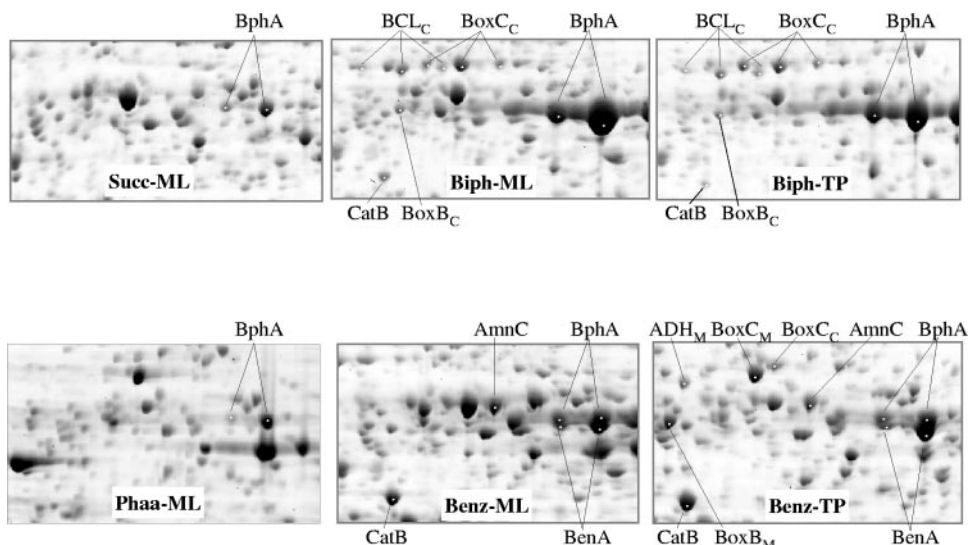


FIG. 2. Sections of 2D gels showing parts of the *B. xenovorans* LB400 cellular proteome. Corresponding gel sections are shown from cells in each of the six different physiological conditions tested. The section was chosen to include protein spots from each of the pathways of interest, including the three benzoate pathways and the biphenyl pathway.

just failed the criteria. The latter are presented in supplementary Table S1 and are not further discussed here. The identified proteins include those of the *box_M* pathway that were picked from 2D gels of a deletion mutant of LB400, the $\Delta benABCD\Delta boxAB_C::kan$ mutant, grown on benzoate (Denef et al., submitted). Through matching experiments, such BoxM proteins were identified in wild-type cells under certain conditions, as described below.

Biphenyl, benzoate and other aromatic catabolic enzymes.

Of seven proteins known to be involved in the transformation of biphenyl to benzoate and a pentadienoate, collectively known as the upper *bph* pathway, six were identified on the 2D gels (Table 1). The seventh protein, the 12.1-kDa BphF, is too small to be detected in these studies. BphK (22.4 kDa, pI 5.6), a GST of unconfirmed function, was not identified. Failure to

identify a protein does not imply its absence as ~40% of the protein spots analyzed by mass spectrometry did not yield usable data. The six identified proteins were all detected in cells sampled at each of the five conditions, but were 2- to 16-fold more abundant in biphenyl-grown cells. Moreover, all three proteins of the lower *bph* pathway, catabolizing pentadienoate, were identified and were most abundant in biphenyl-grown cells. One of these three proteins, BphI, was also relatively abundant in Benz-ML and Succ-ML samples.

Proteins from each of the three aerobic benzoate catabolic pathways predicted to occur in LB400 based on genomic sequence analysis (Fig. 1A) were identified. These proteins include eight of 11 proteins of the *ben-cat* pathway, four of eight proteins of the *box_C* pathway, and four of eight proteins of the *box_M* pathway (Table 1). Of the four proteins of the *box_C* and

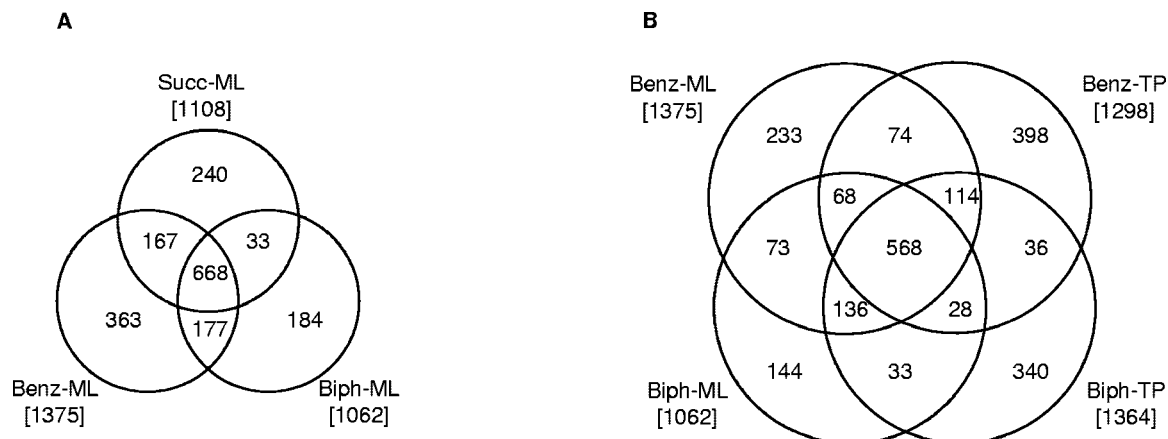


FIG. 3. Venn diagram of the comparative analysis of the cytosolic proteomes of *B. xenovorans* LB400 grown under different conditions. This analysis included only spots detected on pH 3 to 7 gels. Samples were derived from cells at mid-log phase (ML) or transition phase (TP) growing on benzoate, biphenyl, or succinate as the sole source of carbon and energy. The number in parentheses following each condition name indicates the number of protein spots detected on the corresponding average gel. Panel B does not include 109 spots that were only detected in Benz-ML and Biph-TP samples and 12 protein spots that were only detected in Biph-ML and Benz-TP samples.

TABLE 1. Proteins of the aromatic and C₁ metabolic pathways identified by MASCOT-based analysis of MALDI-TOF-generated mass spectra

Protein	MASCOT score ^a	No. of peptides matched	Sequence coverage (%)	Normalized volume ^b				
				Succ-ML	Benz-ML	Benz-TP	Biph-ML	Biph-TP
BphA	115	10	23	1.2	2.1	2.1	15 ^c	11 ^c
BphE	162	10	69	0.71	1.1	1.1	7.6	7.4
BphG	83	13	43	0.08	0.03	0.11	0.26	0.59
BphB	125	10	49	0.13	0.15	0.39	0.77	1.2
BphC	103	15	62	0.12	0.31	0.35	1.9	1.9
BphD	120	8	30	0.16	0.31	0.35	1.5	2.5
BphH	58	5	31	0.02	0.02	0.03	0.25	0.28
BphI	60	8	40	0.10	0.03	0.10	0.29	0.68
BphJ	101	10	46	0.07	0.02	0.03	0.14	0.61
BenA	172	9	29	ND	1.8	1.6	LR ^c	LR ^c
BenB	60	6	45	ND	0.55	1.1	0.12	0.02
BenC	102	9	32	ND	0.26	0.34	0.05	0.01
BenD	68	9	38	ND	0.29	1.2	0.08	0.05
CatA	62	7	29	ND	0.24	2.5	0.25	0.33
CatB	90	10	28	ND	0.59	1.1	0.29	0.12
PcaF	105	16	45	ND	0.57	LR	0.14	0.08
PcaJ	55	5	28	ND	0.26	0.61	0.07	0.04
Benzoate-CoA ligase _C	90	9	24	ND	ND	ND	0.51	0.61
BoxB _C	225	22	54	ND	ND	0.03	0.20	0.22
BoxC _C	247	19	51	ND	ND	0.13	0.71	0.63
Aldehyde dehydrogenase _C	121	19	39	ND	ND	ND	0.13	0.35
Benzoate-CoA ligase _M	71	12	22	ND	ND	0.07	ND	ND
BoxB _M	162	18	37	ND	ND	0.47	ND	ND
BoxC _M	188	25	61	ND	ND	0.78	ND	ND
Aldehyde dehydrogenase _M	100	14	33	ND	ND	0.12	ND	ND
ClcA	56	6	29	ND	0.05	0.21	0.01	0.01
AmnC	78	11	26	ND	0.68	0.47	0.11	0.12
AmnD	57	5	29	ND	0.41	0.26	ND	ND
AmnH	55	8	35	ND	0.05	0.03	ND	0.01
XoxF	157	19	40	ND	ND	ND	ND	0.71
Fae	90	5	49	ND	ND	ND	0.01	0.65
PqqC	65	7	30	ND	ND	ND	ND	0.51

^a MASCOT-generated probability-based Mowse score. In the LB400 protein database scores greater than 52 are significant ($P < 0.05$).

^b Average normalized volumes over the three biological replicates under each of the tested growth conditions. LR, low resolution in area where spot was expected. ND, not detected.

^c Because of their almost identical pI and mass, BenA (pH 5.99 and 52.6 kDa) and BphA (pH 5.99 and 51.9 kDa) were not well resolved on the 2D gel. Due to their relative abundance, separate spots were resolved on gels of the benzoate-grown samples but not on gels of the biphenyl-grown samples. However, levels of BenB in biphenyl-grown samples together with relative levels of BenA and BenB in benzoate-grown samples indicate that BenA constituted less than 5% of the signal of the BphA spot in biphenyl-grown samples.

box_M pathways not identified on the gel, Orf8 was too small (16.7 kDa) to be detected, while Orf10 (a putative transcriptional regulator) was probably present at very low levels, as shown by earlier transcriptomic data (8). Interestingly, none of these four proteins were detected in proteomic analyses of this pathway in *Azoarcus evansii* (9). Of the three unidentified proteins of the *ben-cat* pathway, CatC (11.2 kDa) was too small and PcaI was too basic (pI 7.9) to be detected. Like BphK, PcaD (28.5 kDa, pI 6.1) might be present on the gels but was not identified.

Due to the similarities in the reactions of the *box* and *paa* pathways (9), we investigated whether either of the *box* pathways identified herein might also be involved in phenylacetate catabolism. As summarized in Fig. 2, mid-log-phase cells growing on phenylacetate (Phaa-ML) contained Bph proteins but did not contain detectable amounts of Box, Ben, or Cat protein. A protein in the Phaa-ML sample whose mass and pI are similar to that of BoxC was confirmed not to be the latter by mass spectrometry (results not shown). This result further confirms the identity of the *box* pathways.

Overall, the benzoate catabolic enzymes seemed to be more tightly regulated than the *bph* pathway enzymes. For example, none of former was detected in succinate-grown cells. Moreover, of the three benzoate pathways, Benz-ML cells only contained proteins of the *ben-cat* pathway whereas Benz-TP cells also contained the *Box_M* enzymes. By contrast, cells growing on biphenyl contained the Ben-Cat and *Box_C* but not *Box_M* protein during both tested growth phases (Table 1, Fig. 1, 2, and 4). To better estimate the levels of each of the three benzoate pathways under each of the conditions studied, the normalized volumes of the protein spots were corrected for their mass (NV_C). In the Benz-TP samples, *Box_M* proteins were present at 10 to 20% of the *ben-cat* pathway protein levels. In contrast, the *Box_C* proteins were approximately twice as abundant as the Ben-Cat proteins in biphenyl-grown cells. Finally, Benz-ML samples contained fourfold higher levels of the Ben-Cat proteins than Biph-ML samples on average (Fig. 1A). For TP samples, the difference was even higher: 24-fold.

A number of proteins involved in the catabolism of other aromatic compounds were also detected. Benzoate-grown cells

TABLE 2. Identified proteins involved in cellular processes outside of aromatic and C₁ catabolism^a

Functional class	Annotation (EC number)	Specific function ^b	Gene	Score ^c	#P ^d	SC ^d	Normalized volume ^e				
							Succ-ML	Benz-ML	Benz-TP	Biph-ML	Biph-TP
Stress response	AhpC alkyl hydroperoxide reductase (1.11.1.7)	Detoxification of organic hydroperoxides	2448	118	10	68	0.07	0.10	0.03	0.25	0.20
Stress response	AhpF alkyl hydroperoxide reductase (1.8.1.9)	Detoxification of organic hydroperoxides	2449	86	9	29	0.05	<u>0.07</u>	0.02	0.15	0.05
Stress response	GroEL chaperonin	Involved in degradation of abnormal proteins	7732	142	13	30	6.1	10	6.1	9.9	6.0
Stress response	Heat shock protein HsIU	Proteolysis of abnormal proteins	8238	53	8	18	0.06	0.25	0.20	0.18	0.08
Stress response	Stringent starvation protein A	Unknown	4794	61	7	53	ND	0.08	LR	0.25	0.15
Stress response	PrkA serine kinase	Regulation	6208	109	12	18	0.02	ND	0.16	0.03	0.12
Purine metabolism	PurF (2.4.2.14)	PRPP + Gln → 5'-phosphoribosylamine + Glu	3945	85	14	30	ND	0.03	0.04	0.01	0.01
Purine metabolism	PurA (6.3.4.4)	GTP + IMP = L-aspartate → GDP + phosphate + N(6)-(1,2-dicarboxyethyl)-AMP	5861	74	8	25	0.09	0.24	0.15	0.13	0.01
Amino acid metabolism	Aspartyl tRNA synthetase (6.1.1.12)	Asp + tRNA → Asp-tRNA	7923	61	7	15	ND	0.09	ND	0.05	ND
Amino acid metabolism	Glutamine synthetase (6.3.1.2)	ATP + Glu → ADP + Gln	5786	110	12	30	0.19	0.22	LR	0.42	LR
Amino acid metabolism	Aspartate transaminase (2.6.1.1)	2-Oxoglutarate + Asp → oxaloacetate + Glu	7794	71	11	24	ND	0.01	0.01	ND	0.12
Amino acid metabolism	Histidyl-tRNA synthetase (6.1.1.21)	His + tRNA → His-tRNA	5852	55	11	28	ND	0.13	0.09	0.09	0.05
Amino acid metabolism	IhxC ketol-acid reductoisomerase (1.1.1.86)	2,3-dihydro-3-methylbutanoate → 2-OH-2-methyl-3-oxobutanoate	7236	67	7	26	0.15	0.41	LR	0.18	0.02
Aminosugar metabolism	N-Acetylglucosamine-6-P deacetylase (3.5.1.25)	N-Acetylglucosamine-6-P → D-glucosamine-6-P + acetate	8032	80	8	28	ND	0.04	0.09	ND	ND
Outer membrane protein	Porin (OmpC)	Outer membrane permeability	2049	114	8	40	0.02	0.02	0.04	0.08	0.87
Protein biosynthesis	Ribosomal protein L1	Structural constituent of ribosome	4689	56	5	24	LR	LR	LR	0.12	LR
Outer membrane protein	Porin	Outer membrane permeability	7389	157	14	61	0.01	ND	ND	0.02	0.50
Outer membrane protein	Porin (OmpC)	Outer membrane permeability	4849	121	10	32	0.03	ND	ND	ND	9.6
TCA cycle	Isocitrate dehydrogenase (1.1.1.42)	Isocitrate → 2-oxoglutarate + CO ₂	5150	71	13	31	0.10	0.05	0.29	0.06	0.17
TCA cycle	Citrate synthase (1.7.99.5)	Oxaloacetate + acetyl CoA → citrate + CoA	2385	109	12	32	0.08	1.3	0.66	ND	ND
Fatty acid metabolism	Acetyl-CoA carboxylase, alpha subunit (6.4.1.2)	ATP + acetyl-CoA + HCO ₃ → malonyl-CoA	5882	59	7	32	LR	0.04	LR	0.02	0.01
Fatty acid metabolism	Hypothetical dehydrogenase (1.1.1.100)	3-OH-acyl-ACP → 3-oxoacyl-ACP	6307	66	5	33	0.01	0.04	0.14	0.02	0.02
Fatty acid metabolism	Acyltransferase	Acyl-carrier + reactant = acyl-reactant + carrier	6659	61	6	40	0.01	0.03	0.01	0.21	0.20
DNA replication	DNA polymerase III, beta subunit (2.7.7.7)	Deoxynucleoside triphosphate + DNA(n) = diphosphate + DNA(n+1)	8311	120	18	58	ND	0.14	0.27	0.11	0.11
Other	5,10 methylene THF reductase (1.7.99.5)	5-methyl-THF → 5,10-methylene-THF	4607	69	7	38	LR	0.05	LR	0.01	0.04
Other	Phasin (granule-associated protein)	Unknown	5805	79	7	43	ND	ND	ND	0.04	0.02
Other	Putative Amidase (3.5.1.4)	Monocarboxylic acid amide → monocarboxylate + NH ₃	0365	58	7	22	ND	0.16	0.23	0.03	0.03
Other	Acyl-carrier protein (ACP) phosphodiesterase (3.1.4.14)	ACP + H ₂ O → 4-P-pantetheine + apoprotein	4830	101	6	44	0.005	0.01	0.10	0.16	0.36
Other	Hypothetical hydrolase	Unknown	4637	113	8	34	ND	0.10	0.04	0.09	0.03

^a Abbreviations are as used in Table 1, plus: TCA, tricarboxylic acid; P, phosphate; PRPP, 5-phosphoribosyl 1-pyrophosphate; diOH, dihydroxy; ACP, acyl carrier protein. Normalized volumes in boldface type were at least twofold higher than in control samples (Succ-ML; Progenesis analysis, $P < 0.05$). Singly and doubly underlined values indicate significant up- and down-regulation, respectively, of the corresponding transcript in previous microarray experiments (Genespring; Silicon Genomics); Student *t* test, $P < 0.10$ (8). No microarray data were available for genes 2448, 5150, or 5805 or for any gene in Benz-TP samples.

^b For enzymes, the reaction catalyzed is indicated.

^c Probability-based Mowse score generated by MASCOT. In the LB400 protein database, scores greater than 52 are significant ($P < 0.05$).

^d Number of peptides matched (#P) and sequence coverage (SC) in MASCOT analysis.

^e Average normalized volumes over the three biological replicates under each of the tested growth conditions.

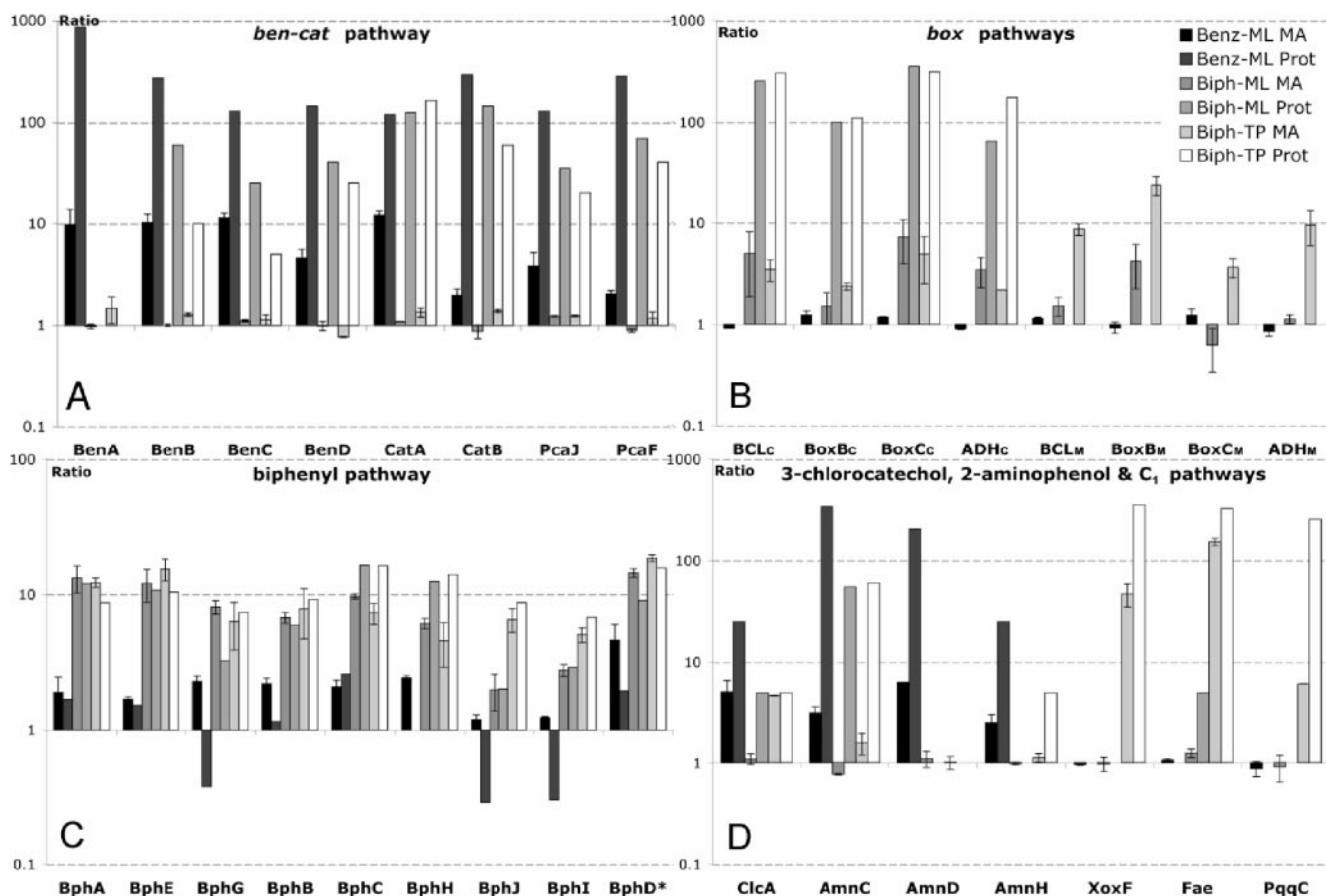


FIG. 4. Comparison of transcript (MA) and protein (Prot) levels for the identified proteins of the following pathways: (A) *ben-cat*; (B) *box_C* and *box_M*; (C) *bph*; and (D) 3-chlorocatechol, 2-aminophenol, and *C₁* catabolism. All levels are relative to those in cells growing exponentially on succinate (control). Transcriptomic data are from Deneff et al. (9, 26, 39, 40). Relative protein levels were calculated as the ratio of normalized volumes. The latter was set to 0.002 when no spot was detected in the control condition. Error bars indicate the standard error between biological replicates. Since transcript data for *bphD* were missing in the microarray data sets, quantitative reverse transcription-PCR data were used (9, 26, 39, 40). See comments on BphA and BenA in Table 1 footnotes.

contained chlorocatechol dioxygenase (ClcA), one of four proteins of the 3-chlorocatechol pathway, as well as three out of eight proteins of the 2-aminophenol pathway (Table 1). Some of these proteins were also detected at lower levels in biphenyl-grown cells. The observed expression patterns of these pathways are consistent with transcriptomic data (Fig. 4).

***C₁* metabolism.** Three proteins of a *C₁* metabolic pathway that potentially catalyzes the oxidation of methanol or methoxy groups to CO_2 were identified: XoxF, a homolog of the large subunit of methanol dehydrogenase; PqqC, one of the enzymes involved in the biosynthesis of pyrroloquinoline quinone, a cofactor of methanol dehydrogenase; and Fae, a formaldehyde-activating enzyme, involved in the tetrahydromethanopterin-dependent oxidation of formaldehyde (Fig. 5). All three proteins were present in Biph-TP samples. None were detected under any other condition except for Fae, small amounts of which were also present in Biph-ML cells (Table 1). The occurrence of these proteins solely in Biph-TP samples is consistent with our transcriptomics data (Fig. 4).

Other cellular functions. We identified 29 other proteins involved in a range of cellular functions. Of these proteins, those that were most abundant in either benzoate- or biphenyl-grown

cells were involved in either oxidative stress response or the metabolism of amino acids, especially aspartate and glutamate (Table 2). The protein identified as GroEL, the large subunit of the main chaperonin, is highly abundant under all conditions. This is consistent with the high hybridization signals in microarray studies (data not shown). However, GroEL is most abundant during mid-log growth on benzoate and biphenyl. Finally, three porins were also detected, but only in Biph-TP samples. Although the detection of porins, which regulate outer membrane permeability, in the cytosolic fraction is unexpected, the quality of the mass spectrometric data (large number of peptides and percent coverage) indicates that the protein spots were correctly identified. The porin peptides identified by mass spectrometry did not include sequences that cover the N-terminal signal peptides predicted from the genomic sequence. Moreover, the mass and pI of each porin estimated from the gels are consistent with the cleavage of their signal peptides.

DISCUSSION

This detailed proteomics study of *B. xenovorans* LB400 enabled us to unambiguously identify the major catabolic path-

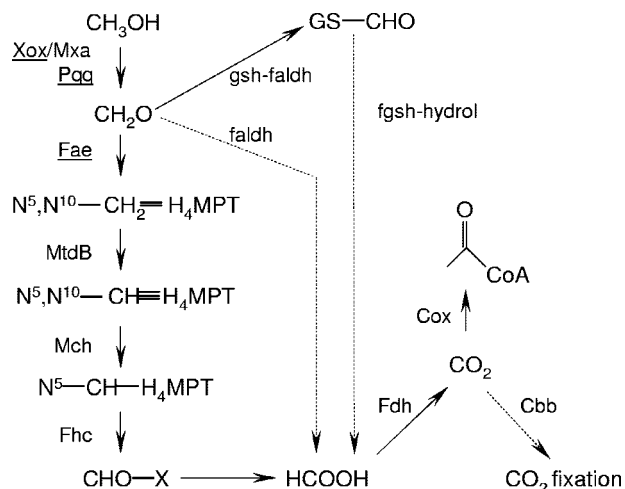


FIG. 5. C_1 metabolic pathways of *B. xenovorans* LB400. The pathways are predicted from the genome sequence. Genes are named as in *Methylobacterium extorquens* (8), except for the glutathione-dependent and -independent formaldehyde dehydrogenases (gsh-faldh and faldh, respectively) and formyl-glutathione hydrolase (fgsh-hydrol). Full lines indicate the corresponding genes that were up-regulated in Biph-TP cells according to microarray experiments (8). Underlined proteins were identified in this study.

ways utilized by the cell when growing on benzoate and biphenyl as sole sources of energy and carbon. More particularly, the data confirm that the *bph* pathway is regulated in LB400 and demonstrate that cells can simultaneously utilize two of three different pathways to catabolize benzoate, depending on their growth state. Thus, although the *ben-cat* pathway was utilized during growth on biphenyl and benzoate, the *Box_C* proteins were more abundant than the Ben-Cat proteins during growth on biphenyl and the *Box_M* proteins were only present during the transition to stationary phase in cells growing on benzoate. These data corroborate and expand previous transcriptomic data which indicated the substrate-dependent utilization of the *ben-cat* and *box_C* pathways. The current data further indicate the involvement of C_1 metabolism in biphenyl-grown cells entering stationary phase.

The occurrence of three benzoate catabolic pathways in LB400 is consistent with functional redundancy observed in this and other large-genome bacteria (23, 33). However, the benefit of having all three pathways, implied by their stable coexistence, is unclear despite their differential expression under different growth conditions. In terms of energetic cost to the cell, the *ben-cat* pathway consists of 11 proteins (2,858 amino acids) and utilizes two molecules of molecular oxygen per molecule of benzoate catabolized. By contrast, the *box* pathway consists of eight proteins (3,318 amino acids) and utilizes one ATP and only one molecule of molecular oxygen per molecule of benzoate (Fig. 1A). These factors are consistent with the cell's preferential utilization of the *ben-cat* pathway during exponential growth in well-aerated benzoate-containing medium, although other factors, such as protein stability and catalytic efficiency, provide additional energetic considerations.

During growth on biphenyl, the activity of the two dioxygenases of the upper *bph* pathway may reduce the level of O_2 in

the cell, which could explain the use of the *box_C* pathway under these conditions. Nevertheless, a proper understanding of the physiological role of the three pathways requires investigation of the pathways' substrate specificities and flux analyses. The latter would establish how much carbon flows through each pathway, which is not possible to infer from the protein levels reported here. Substrate specificities would indicate whether the pathways have different abilities to utilize substituted benzoates or function optimally at different oxygen levels. With respect to the latter point, it is interesting the competition for 3-chlorobenzoate between gentisate and modified *ortho* pathways in two separate bacteria (17). In chemostat experiments performed at high O_2 levels and high dilution rates, the bacterium using the modified *ortho* pathway outcompeted the bacterium using the gentisate pathway. The reverse was true in experiments performed under any one of three other conditions: low dilution rates; low O_2 levels; and high O_2 levels in combination with low 3-chlorobenzoate concentrations. Consistent with these results, the enzymes of the gentisate pathway possessed lower K_m s for O_2 and 3-chlorobenzoate. Thus, enzymes possessing different abilities to utilize oxygen and benzoate would confer a selective advantage on LB400.

The conditional regulation of the three benzoate pathways in LB400 implies a relatively complex regulatory mechanism that might depend on global signals of physiological state in addition to the concentrations of metabolites such as benzoate, molecular oxygen, and/or *cis,cis*-muconate. Sequence analyses indicate that the *ben* and *cat* operons of LB400 are regulated by BenM and CatR, respectively. In other organisms, homologs that share approximately 50% amino acid sequence identity with the LB400 regulators utilize benzoate (29) and *cis,cis*-muconate (32), respectively, as effectors. The concentration of benzoate is higher in benzoate- than in biphenyl-grown cells at the same initial concentrations of these growth substrates. Thus, the increased expression of *ben-cat* genes in benzoate- versus biphenyl-grown cells suggests that this expression is regulated in LB400 as it is in these other organisms. By contrast, the *box* pathway has only recently been described (9, 26, 39, 40) and essentially nothing has been reported about its regulation. The genome sequence of LB400 suggests that transcription of the *box_M* and *box_C* genes is independently regulated by LysR- and TetR-type regulators, respectively. However, the effectors of these two regulators are unknown. Based on our data, the expression of the *box* pathways seems to occur in LB400 only at lower concentrations of benzoate and molecular oxygen.

Overall, the proteomic and transcriptomic data for the catabolic pathways studied herein correspond relatively well with each other (Fig. 4 and Table 1), indicating these pathways are not subject to specific translational control. A notable exception appears to be the lower biphenyl pathway encoded by *bphHJI*: with respect to cells growing on succinate, cells growing on benzoate had higher levels of the transcript(s) but lower levels of the enzyme(s). The mechanism underlying this phenomenon is unclear. The data further indicate interesting relationships between proteins encoded by the same operon. For example, BphB was approximately twofold more abundant in TP versus ML cells, whereas BphC levels remained unchanged, although *bphB* and *bphC* are located adjacent to each other. This may reflect the different rates of proteolysis of the cata-

bolic enzymes as the cell enters stationary phase. Similarly, *boxA* and *boxB* transcripts were detected at similar levels, whereas only the BoxB protein was identified in the current studies. It is possible that the BoxA protein was simply not identified on the gels. However, BoxA was also not detected in proteomic studies of *A. Evansii* (9). Indeed, BoxA appears to be a reductase, delivering electrons to the BoxB oxygenase, and is presumably present at ~30-fold lower levels than BoxB (40). Finally, the conflicting transcriptomic and proteomic data on the *ben-cat* pathway during growth on biphenyl (Fig. 4A) appear to be due to the lack of sensitivity of microarrays, as the up-regulation of *ben-cat* genes was detected using quantitative reverse transcription-PCR (8).

An intriguing difference between the *box* gene cluster of *A. Evansii* (9) and the two of LB400 is that the latter lack genes encoding a β -ketothiolase. This enzyme is thought to catalyze the last step of the pathway, transforming 3-oxoadipyl-CoA to succinyl-CoA and acetyl-CoA. PcaF catalyzes this reaction in the β -ketoacid pathway (Fig. 1A) (13). The LB400 genome is predicted to encode 17 thiolases, including PcaF and four other β -ketothiolases. Sequence analysis indicates that *pcaF* appears to occur as a single-gene operon in LB400 and is separated from all other β -ketoacid pathway genes by ~1.6 Mb. The expression of *pcaF* strongly correlated with that of the *ben-cat* genes (Table 1) (8). In contrast, the expression of none of the 17 predicted thiolase genes correlated with that of the *boxC* genes. Nevertheless, some of the thiolase genes, including those involved in fatty acid metabolism, were expressed under all conditions studied. Any one of these could potentially perform the final step of the *box* pathway in LB400.

The proteomic data confirm the unexpected observation from transcriptomic studies (8) that a C_1 metabolic pathway is present in biphenyl-grown cells during the transition phase. This pathway oxidizes methanol or a methoxy group to CO_2 via formaldehyde in a tetrahydromethanopterin-dependent manner (23, 37, 42). Failure to observe the C_1 metabolic proteins in transition-phase benzoate-grown cells indicates that these proteins are not part of a general response to scavenge less favorable energy sources. It is possible that the C_1 pathway is linked to the transition phase of biphenyl-grown cells and/or induced by a biphenyl catabolite. Consistent with this possibility, one of the proteins, Fae, was present at low levels in mid-log biphenyl-grown cells.

A further interesting observation was the detection of three porins in the proteome of transition phase biphenyl-grown cells. Data derived from a microarray containing probes for 90 of the 96 predicted porin genes of LB400 indicate that four porin genes are up-regulated during transition-phase growth on biphenyl (8), including one of the detected porins (or7389). The latter was also up-regulated in Biph-ML cells but to a lesser extent. Genes for the two other porins detected on 2D gels, or2049 and or4849, were not significantly differentially expressed on the transcript level, but high signals were detected for or4849 under all conditions tested. The genomic context of the genes of the three porins detected here provides no direct clue as to the physiological function of these proteins. The increased abundance of porins in transition phase is not unexpected, as two of the environmental factors that influence their expression are nutrient limitation and cell density (19, 20). Nevertheless, they represent a further unique feature of

the transition phase of biphenyl-grown cells, together with the unusual length of this phase and the C_1 metabolism.

The proteomics analysis also identified a number of non-catabolic proteins apparently associated with aerobic aromatic metabolism, consistent with previous transcriptomic profiles (8). Many of the noncatabolic proteins that were more abundant during growth on biphenyl and/or benzoate versus succinate appear to be associated with a stress response. Oxidative stress may originate from the dioxygenases' activity, which can produce reactive oxygen species (5, 36). Four proteins that were more abundant during growth on the aromatic compounds have been linked to oxidative stress responses: the general stress protein GroEL (5, 6, 15); HslU (25), which degrades abnormal proteins; and AhpCF (4, 21, 31), which detoxifies peroxides; and a serine kinase (38). Moreover, the increases in purine nucleotide metabolism (PurF and 5,10-methylene-THF reductase) may be an indirect response to oxidative damage. Purine nucleotides are more susceptible to oxidative damage than pyrimidine nucleotides, and the biosynthesis genes of the former are up-regulated in response to oxidative stress in higher organisms (18). Other enzymes that were more abundant during growth on biphenyl and benzoate may also be linked to the synthesis of purine building blocks and precursors, including those involved in aspartate and glutamine metabolism and two tricarboxylic acid enzymes, isocitrate dehydrogenase and citrate synthase. Interestingly, enzymes of nucleotide, amino acid, and fatty acid metabolism were more abundant in *Rhodococcus* sp. strain RHA1 during growth on benzoate or phthalate (30).

The transcriptomics and proteomics studies of biphenyl and benzoate catabolism in LB400 provide important insights into the coordinated utilization of multiple catabolic pathways by this large-genome bacterium as well as into the general physiological adaptation of the strain to aromatic growth substrates. These studies also provide a strong basis for investigating the superior PCB-degrading properties of LB400, particularly the noncatabolic processes that may be important to its tolerating these environmental pollutants.

ACKNOWLEDGMENTS

This work was supported by Genome BC, by Superfund Basic Research Program grant P42 ES 04911-12 from the U.S. National Institute of Environmental Health Sciences, and by the Microbial Genome Program of the U.S. Department of Energy. Vincent Deneff is an aspirant of the Fund for Scientific Research-Flanders, Belgium (FWO-Vlaanderen).

Robert Olafson, Derek Smith, and other members of the Proteomics Centre, University of Victoria, are thanked for assistance with the mass spectrometry. We thank Jacob Parnell for growing some of the cultures.

REFERENCES

1. Bedard, D. L., R. Unterman, L. H. Bopp, M. J. Brennan, M. L. Haberi, and C. Johnson. 1986. Rapid assay for screening and characterizing microorganisms for the ability to degrade polychlorinated biphenyls. *Appl. Environ. Microbiol.* **47**:761-768.
2. Beltrametti, F., D. Reniero, S. Backhaus, and B. Hofer. 2001. Analysis of transcription of the *bph* locus of *Burkholderia* sp. strain LB400 and evidence that the ORF0 gene product acts as a regulator of the *bphA1* promoter. *Microbiology* **147**:2169-2182.
3. Bopp, L. H. 1986. Degradation of highly chlorinated PCBs by *Pseudomonas* strain LB400. *J. Ind. Microbiol.* **1**:23-29.
4. Bsat, N., L. Chen, and J. D. Helmann. 1996. Mutation of the *Bacillus subtilis* alkyl hydroperoxide reductase (*ahpCF*) operon reveals compensatory interactions among hydrogen peroxide stress genes. *J. Bacteriol.* **178**:6579-6586.

5. Chavez, F. P., H. Lunsdorf, and C. A. Jerez. 2004. Growth of polychlorinated biphenyl-degrading bacteria in the presence of biphenyl and chlorobiphenyls generates oxidative stress and massive accumulation of inorganic polyphosphate. *Appl. Environ. Microbiol.* **70**:3064–3072.
6. Cho, Y.-S., S.-H. Park, C.-K. Kim, and K.-H. Oh. 2000. Induction of Stress shock proteins DnaK and GroEL by phenoxyherbicide 2,4-D in *Burkholderia* sp. YK-2 isolated from rice field. *Curr. Microbiol.* **41**:33–38.
7. Dai, S., F. H. Vaillancourt, H. Maaroufi, N. M. Drouin, D. B. Neau, V. Snieckus, J. T. Bolin, and L. D. Eltis. 2002. Identification and analysis of a bottleneck in PCB biodegradation. *Nat. Struct. Biol.* **9**:934–939.
8. Denef, V. J., J. Park, T. V. Tsoi, J. M. Rouillard, H. Zhang, J. A. Wibbenmeyer, W. Verstraete, E. Gulari, S. A. Hashsham, and J. M. Tiedje. 2004. Biphenyl and benzoate metabolism in a genomic context: outlining genome-wide metabolic networks in *Burkholderia xenovorans* LB400. *Appl. Environ. Microbiol.* **70**:4961–4970.
9. Gescher, J., A. Zaar, M. Mohamed, H. Schagger, and G. Fuchs. 2002. Genes coding for a new pathway of aerobic benzoate metabolism in *Azoarcus evansii*. *J. Bacteriol.* **184**:6301–6315.
10. Gorg, A., C. Obermaier, G. Boguth, A. Harder, B. Scheibe, R. Wildgruber, and W. Weiss. 2000. The current state of two-dimensional electrophoresis with immobilized pH gradients. *Electrophoresis* **21**:1037–1053.
11. Gorg, A., C. Obermaier, G. Boguth, and W. Weiss. 1999. Recent developments in two-dimensional gel electrophoresis with immobilized pH gradients: wide pH gradients up to pH 12, longer separation distances and simplified procedures. *Electrophoresis* **20**:712–717.
12. Goris, J., P. De Vos, J. Caballero-Mellado, J. Park, E. Falsen, J. F. Quensen Spaceiiqq, J. M. Tiedje, and P. Vandamme. 2004. Classification of the PCB- and biphenyl degrading strain LB400 and relatives as *Burkholderia xenovorans* sp. nov. *Int. J. Syst. Evol. Microbiol.* **54**:1677–1681.
13. Harwood, C. S., and R. E. Parales. 1996. The beta-ketoadipate pathway and the biology of self-identity. *Annu. Rev. Microbiol.* **50**:553–590.
14. Hofer, B., L. D. Eltis, D. N. Dowling, and K. N. Timmis. 1993. Genetic analysis of a *Pseudomonas* locus encoding a pathway for biphenyl/polychlorinated biphenyl degradation. *Gene* **130**:47–55.
15. Kandror, O., M. Sherman, and A. Goldberg. 1999. Rapid degradation of an abnormal protein in *Escherichia coli* proceeds through repeated cycles of association with GroEL. *J. Biol. Chem.* **274**:37743–37749.
16. Kinter, M. T., and N. E. Sherman. 2000. Protein sequencing and identification using tandem mass spectrometry. John Wiley & Sons Inc., New York, N.Y.
17. Krooneman, J., E. R. B. Moore, J. C. L. van Velzen, R. A. Prins, L. J. Forney, and J. C. Gottschal. 1998. Competition for oxygen and 3-chlorobenzoate between two aerobic bacteria using different degradation pathways. *FEMS Microbiol. Ecol.* **26**:171–179.
18. Landis, G. N., D. Abdueva, D. Skvortsov, J. Yang, B. E. Rabin, J. Carrick, S. Tavare, and J. Tower. 2004. Similar gene expression patterns characterize aging and oxidative stress in *Drosophila melanogaster*. *Proc. Natl. Acad. Sci. USA* **101**:7663–7668.
19. Liu, X., and T. Ferenci. 1998. Regulation of porin-mediated outer membrane permeability by nutrient limitation in *Escherichia coli*. *J. Bacteriol.* **180**:3917–3922.
20. Liu, X., C. Ng, and T. Ferenci. 2000. Global adaptations resulting from high population densities in *Escherichia coli* cultures. *J. Bacteriol.* **182**:4158–4164.
21. Loprasert, S., R. Sallabhan, W. Whangsuk, and S. Mongkolsuk. 2003. Compensatory increase in *ahpC* gene expression and its role in protecting *Burkholderia pseudomallei* against reactive nitrogen intermediates. *Arch. Microbiol.* **180**:498–502.
22. Maltseva, O. V., T. V. Tsoi, J. F. Quensen Spaceiiqq, M. Fukuda, and J. M. Tiedje. 1999. Degradation of anaerobic reductive dechlorination products of Aroclor 1242 by four aerobic bacteria. *Biodegradation* **10**:363–371.
23. Marx, C. J., J. A. Miller, L. Chistoserdova, and M. E. Lidstrom. 2004. Multiple formaldehyde oxidation/detoxification pathways in *Burkholderia fungorum* LB400. *J. Bacteriol.* **186**:2173–2178.
24. Master, E. R., and W. W. Mohn. 2001. Induction of *bphA*, encoding biphenyl dioxygenase, in two polychlorinated biphenyl-degrading bacteria, psychrotolerant *Pseudomonas* strain Cam-1 and mesophilic *Burkholderia* strain LB400. *Appl. Environ. Microbiol.* **67**:2669–2676.
25. Missiakas, D., F. Schwager, J. M. Betton, C. Georgopoulos, and S. Raina. 1996. Identification and characterization of HsIV HsIU (ClpQ ClpY) proteins involved in overall proteolysis of misfolded proteins in *Escherichia coli*. *EMBO J.* **15**:6899–6909.
26. Mohamed, M. E., A. Zaar, C. Ebenau-Jehle, and G. Fuchs. 2001. Reinvestigation of a new type of aerobic benzoate metabolism in the proteobacterium *Azoarcus evansii*. *J. Bacteriol.* **183**:1899–1908.
27. Mondello, F. J. 1989. Cloning and expression in *Escherichia coli* of *Pseudomonas* strain LB400 genes encoding polychlorinated biphenyl degradation. *J. Bacteriol.* **171**:1725–1732.
28. Moritz, B., and H. E. Meyer. 2003. Approaches for the quantification of protein concentration ratios. *Proteomics* **3**:2208–2220.
29. Neidle, E. L., and L. N. Ornston. 1987. Benzoate and muconate, structurally dissimilar metabolites, induce expression of *catA* in *Acinetobacter calcoaceticus*. *J. Bacteriol.* **169**:414–415.
30. Patrauchan, M. A., C. Florizone, M. Dosanjh, W. W. Mohn, J. Davies, and L. D. Eltis. 2005. Catabolism of benzoate and phthalate in *Rhodococcus* sp. strain RHA1: redundancies and convergence. *J. Bacteriol.* **187**:4050–4063.
31. Poole, L. B., and H. R. Ellis. 1996. Flavin-dependent alkyl hydroperoxide reductase from *Salmonella typhimurium*. 1. Purification and enzymatic activities of overexpressed AhpF and AhpC proteins. *Biochemistry* **35**:65–75.
32. Rothmel, R. K., T. L. Aldrich, J. E. Houghton, W. M. Coco, L. N. Ornston, and A. M. Chakrabarty. 1990. Nucleotide sequencing and characterization of *Pseudomonas putida catR*: a positive regulator of the *catBC* operon is a member of the LysR family. *J. Bacteriol.* **172**:922–931.
33. Sakai, M., E. Masai, H. Asami, K. Sugiyama, K. Kimbara, and M. Fukuda. 2002. Diversity of 2,3-dihydroxybiphenyl dioxygenase genes in a strong PCB degrader, *Rhodococcus* sp. strain RHA1. *J. Biosci. Bioeng.* **93**:421–427.
34. Seah, S. Y. K., G. Labbé, S. Nerdinger, M. R. Johnson, V. Snieckus, and L. D. Eltis. 2000. Identification of a serine hydrolase as a key determinant in the microbial degradation of polychlorinated biphenyls. *J. Biol. Chem.* **275**:15701–15708.
35. Seeger, M., M. Zielinski, K. N. Timmis, and B. Hofer. 1999. Regiospecificity of dioxygenation of di- to pentachlorobiphenyls and their degradation to chlorobenzoates by the *bph*-encoded catabolic pathway of *Burkholderia* sp. strain LB400. *Appl. Environ. Microbiol.* **65**:3614–3621.
36. Tamburro, A., I. Robuffo, H. J. Heipieper, N. Allocati, D. Rotilio, C. Di Ilio, and B. Favaloro. 2004. Expression of glutathione S-transferase and peptide methionine sulphoxide reductase in *Ochrobactrum anthropi* is correlated to the production of reactive oxygen species caused by aromatic substrates. *FEMS Microbiol. Lett.* **241**:151–156.
37. Vorholt, J. A. 2002. Cofactor-dependent pathways of formaldehyde oxidation in methylotrophic bacteria. *Arch. Microbiol.* **178**:239–249.
38. Xu, W.-L., R. Jeanjean, Y.-D. Liu, and C.-C. Zhang. 2003. *pkn22* (*ahr2502*) encoding a putative Ser/Thr kinase in the cyanobacterium *Anabaena* sp. PCC 7120 is induced by both iron starvation and oxidative stress and regulates the expression of *isiA*. *FEBS Lett.* **553**:179–882.
39. Zaar, A., W. Eisenreich, A. Bacher, and G. Fuchs. 2001. A novel pathway of aerobic benzoate catabolism in the bacteria *Azoarcus evansii* and *Bacillus stearothermophilus*. *J. Biol. Chem.* **276**:24997–25004.
40. Zaar, A., J. Gescher, W. Eisenreich, A. Bacher, and G. Fuchs. 2004. New enzymes involved in aerobic benzoate metabolism in *Azoarcus evansii*. *Mol. Microbiol.* **54**:223–238.
41. Zaitsev, G. M., and Y. N. Karasevich. 1985. Primary steps in metabolism of 4-chlorobenzoate in *Arthrobacter globiformis*. *Mikrobiologiya* **50**:423–428.
42. Zhang, M., and M. E. Lidstrom. 2003. Promoters and transcripts for genes involved in methanol oxidation in *Methylobacterium extorquens* AM1. *Microbiology* **149**:1033–1040.
43. Zielinski, M., S. Kahl, H. J. Hecht, and B. Hofer. 2003. Pinpointing biphenyl dioxygenase residues that are crucial for substrate interaction. *J. Bacteriol.* **185**:6976–6980.